J. Am. Soc. Mass Spectrom. (2016)
DOI: 10.1007/s13361-016-1351-y

RESEARCH ARTICLE

Analysis of Supramolecular Complexes of 3-Methylxanthine with Field Asymmetric Waveform Ion Mobility Spectrometry Combined with Mass Spectrometry

Kayleigh L. Arthur,[1] Gary A. Eiceman,[1,2] James C. Reynolds,[1] Colin S. Creaser[1]

[1]Center for Analytical Science, Department of Chemistry, Loughborough University, Loughborough, LE11 3TU, UK
[2]Department of Chemistry and Biochemistry, New Mexico State University, MSC 3C, P.O. Box 3001, Las Cruces, NM 88003-8001, USA

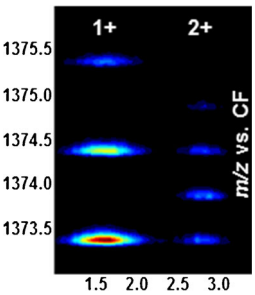

Abstract. Miniaturised field asymmetric waveform ion mobility spectrometry (FAIMS), combined with mass spectrometry (MS), has been applied to the study of self-assembling, noncovalent supramolecular complexes of 3-methylxanthine (3-MX) in the gas phase. 3-MX forms stable tetrameric complexes around an alkali metal (Na^+, K^+) or ammonium cation, to generate a diverse array of complexes with single and multiple charge states. Complexes of $(3\text{-MX})_n$ observed include: singly charged complexes where n = 1–8 and 12 and doubly charged complexes where n = 12–24. The most intense ions are those associated with multiples of tetrameric units, where n = 4, 8, 12, 16, 20, 24. The effect of dispersion field on the ion intensities of the self-assembled complexes indicates some fragmentation of higher order complexes within the FAIMS electrodes (in-FAIMS dissociation), as well as in-source collision induced dissociation within the mass spectrometer. FAIMS-MS enables charge state separation of supramolecular complexes of 3-MX and is shown to be capable of separating species with overlapping mass-to-charge ratios. FAIMS selected transmission also results in an improvement in signal-to-noise ratio for low intensity complexes and enables the visualization of species undetectable without FAIMS.

Keywords: Field asymmetric waveform ion mobility spectrometry, FAIMS, Mass spectrometry, Self-assembling complexes, Dissociation, In-source CID, Charge state separation

Received: 18 December 2015/Revised: 22 January 2016/Accepted: 23 January 2016

Introduction

Self-assembling supramolecular complexes of simple molecules are of interest in a wide variety of fields [1], including structural biology [2], self-assembling membranes [3], therapeutic delivery systems [4], nanostructures [5–7], electrochemistry [8], and supramolecular technology [9]. 3-Methylxanthine (3-MX) is an example of a small molecule that can form stable noncovalently bound supramolecular complexes in the gas phase [10]. 3-MX has been shown to self-assemble in the presence of alkali metals and ammonium ions to form clusters around a stabilizing cation, as shown in Structure1; the 3-MX purine base contains both hydrogen bond donor [NH(1) and O(2)) and acceptor (NH(7) and O(6)] groups [11–13].

3-MX is a purine derivative and a metabolite of caffeine and theophylline [14, 15], and has been monitored biologically in urine and plasma by liquid chromatographic methods [16–19]. Guanine is a related purine base structure that self-assembles into tetrad structures in biological systems (G-quadruplexes) to form complexes that have been well characterized, theoretically and experimentally [2, 20–24]. Other related purine bases, such as xanthine and uric acid derivatives, have shown to similarly self-assemble into noncovalently bound tetrameric species [11, 25, 26]. G-quadruplexes are of significant interest because of their formation in vivo at telomeres and their potential application as anticancer drug targets. Purine bases such as xanthine and uric acid are an intermediate and the end product, respectively, of purine metabolism, which are of interest in the analysis of metabolites, as elevated levels can lead to a number of diseases and conditions [25].

Electronic supplementary material The online version of this article (doi:10.1007/s13361-016-1351-y) contains supplementary material, which is available to authorized users.

Correspondence to: James C. Reynolds; *e-mail:* J.C.Reynolds@lboro.ac.uk, Colin S. Creaser; *e-mail:* C.S.Creaser@lboro.ac.uk

Published online: 25 February 2016

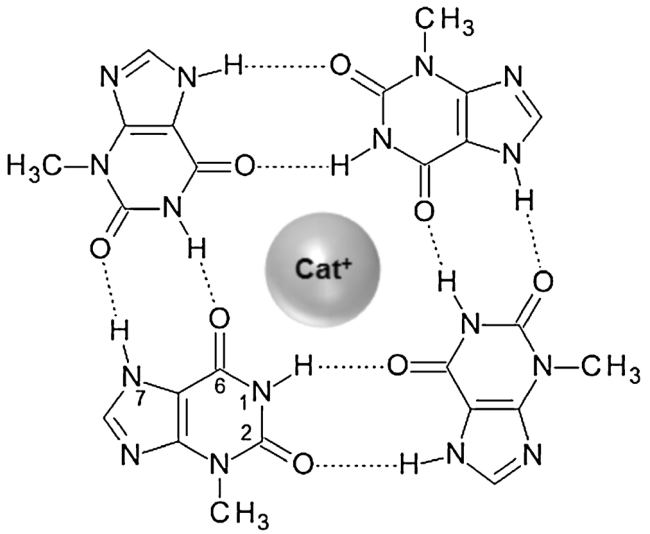

Structure 1. Proposed structure of 3-MX noncovalently bound tetramer ($[(3\text{-MX})_4 + Cat]^+$) with stabilising cation ($cat^+ = NH_4^+$, Na^+, or K^+) [10, 12, 13]

Ion mobility spectrometry (IMS) is an ion separation technique that distinguishes ions based upon their velocity as they migrate through a buffer gas under the influence a weak electric field, where ion mobility is determined by the ratio of the velocity of the ion to the applied electric field. Under strong electric fields, the mobility of an ion has a nonlinear dependence on the electric field strength, and this forms the basis of field asymmetric waveform ion mobility spectrometry (FAIMS), which separates ions based upon the compound-dependent differences in their mobilities in alternating high and low electric fields. In a FAIMS device, ions pass between two electrodes with an applied asymmetric RF waveform known as the dispersion field (DF), under which the ions experience alternating low and high fields, resulting in a net displacement towards one of the electrodes [27–31]. A small DC voltage, known as the compensation field (CF), is superimposed on the DF to transmit selected analytes by offsetting the net displacement through the device [32–34] The DF and CF [unit of Townsend (Td) where 1 Td = 10^{-17} V cm^{-2}] can be scanned over a range to produce a two-dimensional FAIMS spectrum or set statically to transmit ions of interest. The separation of ions based on their mobility under low (<10 Td) and high (>100 Td) field conditions has a high level of orthogonality to mass-to-charge (*m/z*) separation in mass spectrometry (MS) allowing for the hyphenation of FAIMS-MS [35].

3-MX has been studied by electrospray ionization mass spectrometry (ESI-MS) and nuclear magnetic resonance by Szolomájer et al. [10]; mass spectral data for a single tetrameric complex of 3-MX (or tetrad) and an octameric species composed of two parallel tetrads were reported. Here we report a study using ESI combined with a prototype FAIMS device and orthogonal acceleration time-of-flight (TOF) MS, to investigate noncovalently bound, supramolecular complexes of $(3\text{-MX})_n$. Singly charged complexes up to n = 12, doubly charged complexes up to n = 24, and a range of intermediate complexes are observed. This study demonstrates the capability of FAIMS to aid in the analysis of noncovalent supramolecular complexes by mass spectrometry.

Experimental

Sample Preparation

HPLC grade methanol, water, and analytical grade sodium hydroxide and ammonium acetate were purchased from Fisher Scientific (Loughborough, UK). 3-MX was purchased from Sigma-Aldrich (Gillingham, UK). 3-MX (0.5 mM) solutions in 60:40 v/v methanol:water were prepared with two different modifiers (1 mM each): sodium hydroxide and ammonium acetate to promote adduct clusters. Standard solutions of 3-MX were analyzed by direct syringe infusion.

ESI-MS and ESI-FAIMS-MS Instrumentation

ESI-FAIMS-MS analyses were carried out using an Agilent 6230 TOF MS (Agilent Technologies, UK) fitted with a prototype miniaturised chip-based FAIMS (Owlstone Ltd., Cambridge, UK), which has been described in detail elsewhere [33, 36, 37]. The FAIMS device was located behind the modified spray shield of the Jet Stream ESI source, in front of the mass spectrometer inlet capillary, and consists of multiple parallel planar electrode channels (100 µm electrode gap) with a short trench length (78.1 mm) and ion path length (700 µm).

Direct infusion ESI-MS experiments were carried out in positive ionization mode using a 10 µL min^{-1} sample infusion rate from a syringe pump. The ESI nebulizer pressure was set to 30 psig with a sheath gas (N_2) flow of 10 L min^{-1} at 200 °C, with the nozzle voltage set to 2000 V. The capillary voltage was set to 3500 V and the drying gas (N_2) flow to 8 L min^{-1} at 150 °C. The MS scan rate was 10 scans per s in the mass range *m/z* 90–2200, with a fragmentor voltage of 150 V.

ESI-FAIMS-MS experiments were performed by direct syringe infusion of 3-MX solutions and by scanning of the FAIMS DF and CF to investigate the transmission of singly and doubly charged 3-MX clusters through the FAIMS device. The DF was stepped from 194 to 323 Td (12 steps) and the CF was scanned from –2 to +5 Td, at a rate of 0.1 Td s^{-1} (140 steps), to perform a two-dimensional scan of the FAIMS parameters.

Results and Discussion

The self-assembly of 3-MX results in a complex ESI mass spectrum when a solution of 3-MX is infused in 60:40 v/v methanol:water with 1 mM ammonium acetate (Figure 1). A range of noncovalent clusters with different cations are observed in the gas phase, in agreement with Szolomájer et al. [10]. When ammonium acetate is added as a solvent modifier, abundant peaks correspond to tetrameric species with alkali metal and ammonium cations (Figure 1a); for example $[(3\text{-MX})_4 + NH_4]^+$ (*m/z* 682), $[(3\text{-MX})_4 + Na]^+$ (*m/z* 687), and $[(3\text{-MX})_4 + K]^+$ (*m/z* 703). The mass spectrum is characterized

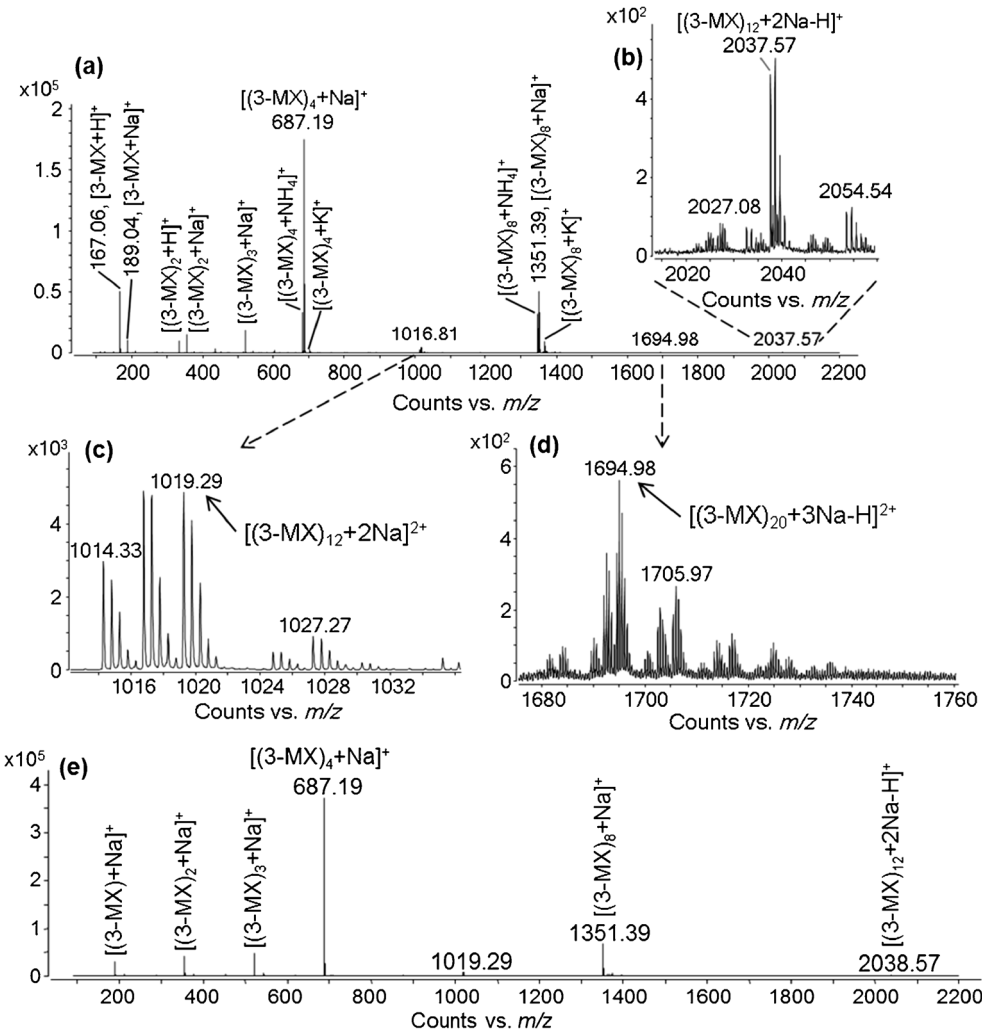

Figure 1. (**a**) Mass spectrum of 3-MX in 60:40 MeOH:H_2O with 1 mM ammonium acetate with FAIMS off; inserts show zoomed in regions of the spectra: (**b**) a mixture of singly and doubly charged species in the region *m/z* 2010–2060, (**c**) doubly charged species in the region *m/z* 1012–1040, (**d**) doubly and multiply charged species in the region *m/z* 1680–1760; (**e**) mass spectrum of 3-MX in 60:40 MeOH:H_2O with 1 mM sodium hydroxide with FAIMS off

by many singly (Figure 1a), doubly (Figure 1b–d), and multiply (Figure 1d) charged species, making it difficult to identify which species are present because of the overlapping isotopic patterns.

The use of sodium hydroxide as a solvent modifier results in a simplified mass spectrum dominated by singly charged sodiated adducts as shown in Figure 1e. The base peak in the spectrum is the $[(3\text{-MX})_4 + Na]^+$ ion at *m/z* 687.19, with the second most intense response corresponding to the $[(3\text{-MX})_8 + Na]^+$ ion at *m/z* 1351.39. Monomer, dimer, and trimer sodiated complexes are observed with lower intensities at *m/z* 189.04, 355.09, and 521.14 respectively, suggesting that the tetrameric based complexes are more stable than non-tetrameric structures. Complexes of $(3\text{-MX})_n$ observed in the presence of sodium ions include: singly charged tetrameric complexes $[(3\text{-MX})_n + xNa - yH]^+$ (x – y = 1 for x = 1–5, y = 0–4) where n = 4, 8, and 12; doubly charged tetrameric complexes $[(3\text{-MX})_n + xNa - yH]^{2+}$ (x – y = 2 for x = 2–10, y= 0–8) where n = 12, 16, 20, and 24; and a range of triply charged complexes corresponding to n = 32 in the region *m/z* 1815–1850, for example $[(3\text{-MX})_{32} + 6Na - 3H]^{3+}$. Intermediate non-tetrameric complexes of low intensity are also observed that correspond to singly charged complexes where n = 1–3 and 5–7, and doubly charged non-tetrameric complexes where n = 13-15 and 17-23. The focus of this study was on the 3-MX monomer and singly charged tetrameric complexes of 3-MX with sodium: $[(3\text{-MX}) + Na]^+$ (*m/z* 189.04), $[(3\text{-MX})_4 + Na]^+$ (*m/z* 687.18), $[(3\text{-MX})_8 + Na]^+$ (*m/z* 1351.38), and $[(3\text{-MX})_{12} + 2Na - H]^+$ (*m/z* 2037.55).

The sodiated 3-MX clusters present in the ESI-MS spectrum (Figure 1) were also observed using ESI-FAIMS-MS. This demonstrates that supramolecular complexes of 3-MX may be transmitted through the FAIMS device in the presence of the alternating high and low electric fields and at a temperature of 150 °C (stand-alone FAIMS is routinely used at much lower temperatures (i.e. atmospheric temperature) [38]. The hyphenation of FAIMS with MS allows ions of a single *m/z* to be selected as the CF is scanned at a fixed DF giving the

characteristic FAIMS CF spectrum of each ion. Alternatively, a FAIMS three-dimensional representation of DF, CF, and intensity can be obtained by sweeping the DF (194–323 Td, in steps of 10 Td) and CF (–2–5 Td, in steps of 0.05 Td) to generate a heat map (or contour plot), where DF is plotted against CF and the intensity is represented by a colour scale [39]. The ESI-FAIMS-MS heat maps are plotted for mass-selected ions in order to provide a way to observe the behaviour of selected ions transmitted through the FAIMS device, and aid in the selection of parameters to resolve ions of interest [39].

The 3-MX monomeric species is the building block of all of the complexes in the mass spectrum for 3-MX (Figure 1). Figure 2 shows the FAIMS characteristics of the 3-MX monomer ($[(3\text{-MX}) + Na]^+$, *m/z* 189.04) at three different fragmentor voltages on the MS, which is applied in the intermediate pressure region of the MS interface, with the FAIMS swept between DF 180–300 Td (steps of 10 Td) and CF –2–5 Td (steps of 0.05 Td). The monomer ion observed at DF 200 Td and fragmentor voltage of 150 V (Figure 2a black solid line, and Figure 2b), is an intense peak centred around CF –0.05 Td can be observed at DF values up to 260 Td, with a secondary peak centred around CF 0.65 Td at DF 200 Td in Figure 2a. This secondary peak can be observed to reduce in intensity as the fragmentor voltage is lowered from 150 to 100 V (Figure 2a. grey dotted line, and Figure 2c), and when lowered to 50 V (Figure 2a grey, solid line, and Figure 2d). The peak is not present in the CF spectrum at DF 200 Td and little remains in the heat map at 50 V. The overlaid CF spectra for the 3-MX dimer ($[(3\text{-MX})_2 + Na]^+$ *m/z* 355.09) in Figure 2b, black dotted line, is also centred around CF 0.65 Td at DF 200 Td, showing a strong correlation to the secondary peak in the CF spectra of the 3-MX monomer. This suggests that the dimer was transmitted through the FAIMS electrodes intact and fragmented in the MS interface by in-source collision induced dissociation (in-source CID) at 150 V post-FAIMS separation, resulting in the two peaks evident in the CF spectra and the FAIMS heat maps for the *m/z* 189.04 [36, 40]. This is further supported by the mass spectra (Supplementary Figure 1) extracted at the optimum FAIMS transmission conditions for the two peaks (DF 200 Td, CF –0.05 Td and 0.65 Td) at each of the three fragmentor voltages, showing the *m/z* 189 ion of the 3-MX monomer present in the mass spectra at CF 0.65 Td at 150 V, which decreases at 100 V and is not present at 50 V. In each of the heat maps for the 3-MX monomer (Figure 2b, c, and d), the intensity reduces sharply as the DF increases above 240 Td, resulting from a greater number and velocity of collisions due to field heating at higher DFs [28, 32].

The change in CF for transmission of the $(3\text{-MX})_n$ (n = 4, 8, 12) tetrameric complexes, in Figure 3a, follows a trend with increased distance from 0 Td in the order: $[(3\text{-MX})_{12} + 2Na - H]^+$ (1.15 Td) < $[(3\text{-MX})_8 + Na]^+$ (1.70 Td) < $[(3\text{-MX})_4 + Na]^+$ (2.05 Td), i.e., the difference in CF from 0 Td decreases as the size of the complex increases. The increased distance from 0 Td can be attributed to increased differences in mobility between electric field extremes. The overlap of the CF spectra and near even distribution of this trend suggests an incremental effect of

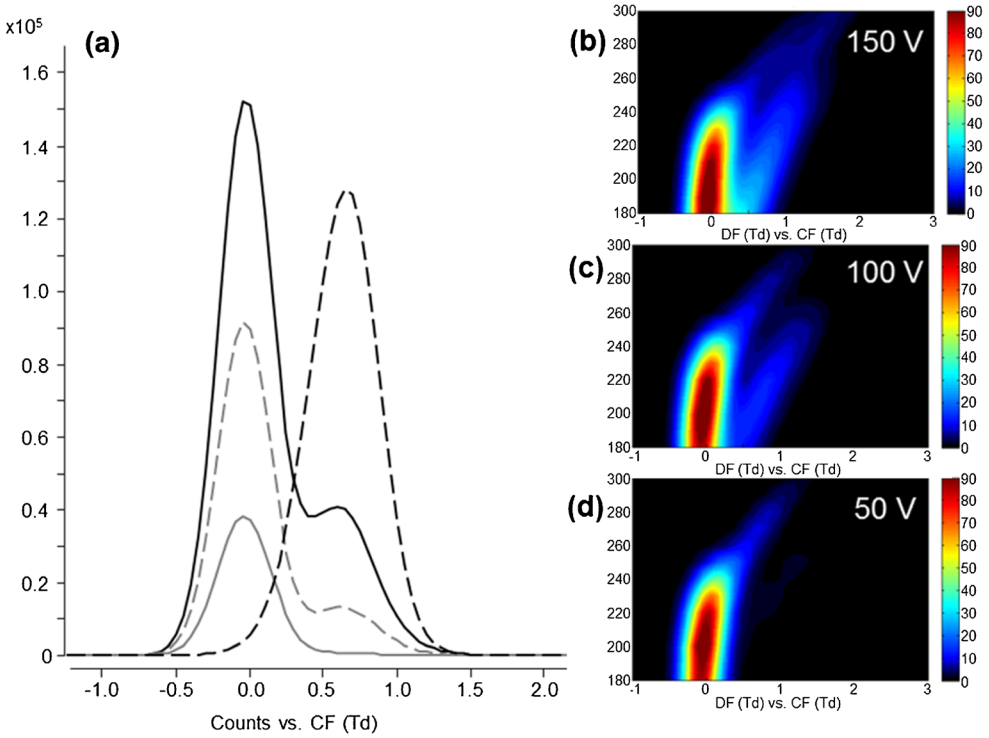

Figure 2. ESI-FAIMS-MS analysis of $[(3\text{-MX}) + Na]^+$ (*m/z* 189.04) at three different MS fragmentor voltages: (**a**) overlaid CF spectra at DF 200 Td where the black solid line = $[(3\text{-MX}) + Na]^+$ at 150 V, grey dotted line = $[(3\text{-MX}) + Na]^+$ at 100 V, grey solid line = $[(3\text{-MX}) + Na]^+$ at 50 V, black dotted line = $[(3\text{-MX})_2 + Na]^+$ (*m/z* 355.09) at 150 V; three-dimensional heat maps of DF versus CF (where intensity (%) is represented on the color scale) of (**b**) *m/z* 189.04 at 150 V, (**c**) *m/z* 189.04 at 100 V, and (**d**) *m/z* 189.04 at 50 V

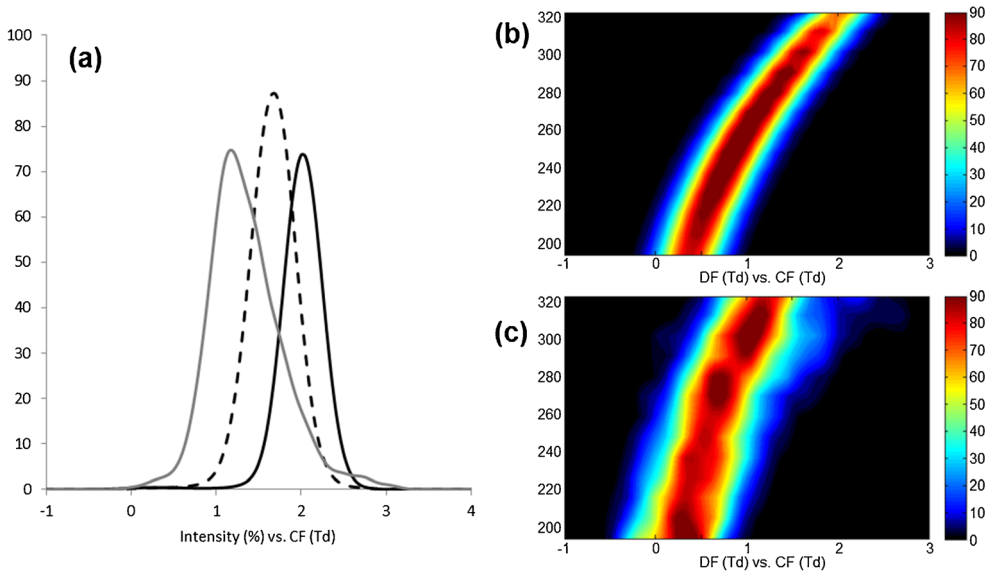

Figure 3. (**a**) CF spectra at DF 323 Td for singly charged sodium doped tetrameric 3-MX complexes: black solid line = $[(3\text{-MX})_4 + Na]^+$ (*m/z* 687.18), black dotted line = $[(3\text{-MX})_8 + Na]^+$ (*m/z* 1351.38), grey solid line = $[(3\text{-MX})_{12} + 2Na - H]^+$ (*m/z* 2037.55); three-dimensional heat maps of DF versus CF (where intensity (%) is represented on the colour scale) of (**b**) $[(3\text{-MX})_4 + Na]^+$ (*m/z* 687.18), and (**c**) $[(3\text{-MX})_{12} + 2Na - H]^+$ (*m/z* 2037.55)

the FAIMS conditions of the tetrameric-based structures of these singly charged complexes of 3-MX, possibly indicating an influence of structure and size, and suggests a relationship with the number of layers in the stacked assembly [5, 10].

The single tetramer structure ($[(3\text{-MX})_4 + Na]^+$, *m/z* 687.18) was observed to be stable through the FAIMS device at all DFs up to 300 Td (Figure 3a solid black line and b), indicated by the symmetrical profile that retains a constant peak width, with a slight fall in intensity at the higher DFs up to 323 Td. In contrast, the $[(3\text{-MX})_{12} + 2Na - H]^+$ (*m/z* 2037.55) ion has a broad, unsymmetrical profile at all DFs (Figure 3c) compared with the single tetramer complex (Figure 3b). This unsymmetrical broadening of the $[(3\text{-MX})_{12} + 2Na - H]^+$ profile (Figure 3c) at DFs above 270 Td could be due to a combination of factors such as: signal instability due to the low intensity of the ion; a higher probability of a distribution of conformations for this larger complex; or the dissociation of higher complexes during transmission through the FAIMS electrodes. Evidence for in-FAIMS dissociation is provided in the mass spectra, shown in Supplementary Figure 2, extracted at DF 323 Td and CF 2.70 Td, corresponding to the high CF tailing edge of the asymmetrical peak of the $[(3\text{-MX})_{12} + 2Na - H]^+$ ion (Figure 3a). In addition to the singly charged *m/z* 2037.55 ion in the mass spectrum (Supplementary Figure 2b), abundant species include higher ordered doubly charged ions of n = 16 and 20 in the regions *m/z* 1362–1395 and *m/z* 1694–1716, respectively. This suggests that the electric field strengths experienced by ions in the FAIMS (up to 60 kV cm^{-1}) may cause higher ordered and doubly charged complexes, such as n = 16, 20, and 24 (formed in the ESI source) to dissociate to yield singly charged *m/z* 2037.55 ions during transmission through the FAIMS electrodes (the relative fragility of the structures can be observed via a tandem MS analysis shown in Supplementary Figure 3).

The singly charged octameric complex, $[(3\text{-MX})_8 + Na]^+$ (Figure 4a), is observed to have a very stable and symmetrical profile even up to the highest DF values, similar to the single tetramer structure $[(3\text{-MX})_4 + Na]^+$ (Figure 3b), but the reduction in ion intensity as the DF increases, expected due to increased field heating and scattering of ions through the FAIMS device at higher DFs, is not observed. The CF for maximum transmission of $[(3\text{-MX})_8 + Na]^+$ increases from 0.35 Td (DF 194 Td) to 1.70 Td (DF 323 Td), an increase of 1.35 Td. In contrast, a doubly charged complex $[(3\text{-MX})_{16} + 3Na - H]^{2+}$ (Figure 4b), whilst having a symmetrical profile, is much more affected by the electric fields with the CF for maximum transmission increasing from 0.65 Td (DF 194 Td) to 2.85 Td (DF 323 Td), an increase of 2.20 Td, and the intensity starts to decrease significantly at DF 260 Td and above. The intensities of $[(3\text{-MX})_8 + Na]^+$ and $[(3\text{-MX})_{16} + 3Na - H]^{2+}$ at DF values in the range 180–300 Td at the lowest fragmentor voltage of 50 V (Supplementary Figure 4), show the expected decrease in the intensity for the doubly charged $[(3\text{-MX})_{16} + 3Na - H]^{2+}$ ion at higher DFs as seen from Figure 4h. However, the intensity of $[(3\text{-MX})_8 + Na]^+$ ion shows an unexpected overall increase as the DF increases. We believe that this increase in intensity of the singly charged 3-MX octameric complex is evidence that the higher ordered and more highly charged species, such as the doubly charged $[(3\text{-MX})_{16} + 3Na - H]^{2+}$, may dissociate in the FAIMS device into the smaller singly charged complexes, such as $[(3\text{-MX})_8 + Na]^+$.

The isotope pattern provides a source of identification for singly or multiply charged species in mass spectrometry, but will not separate isobaric ions of different charge states.

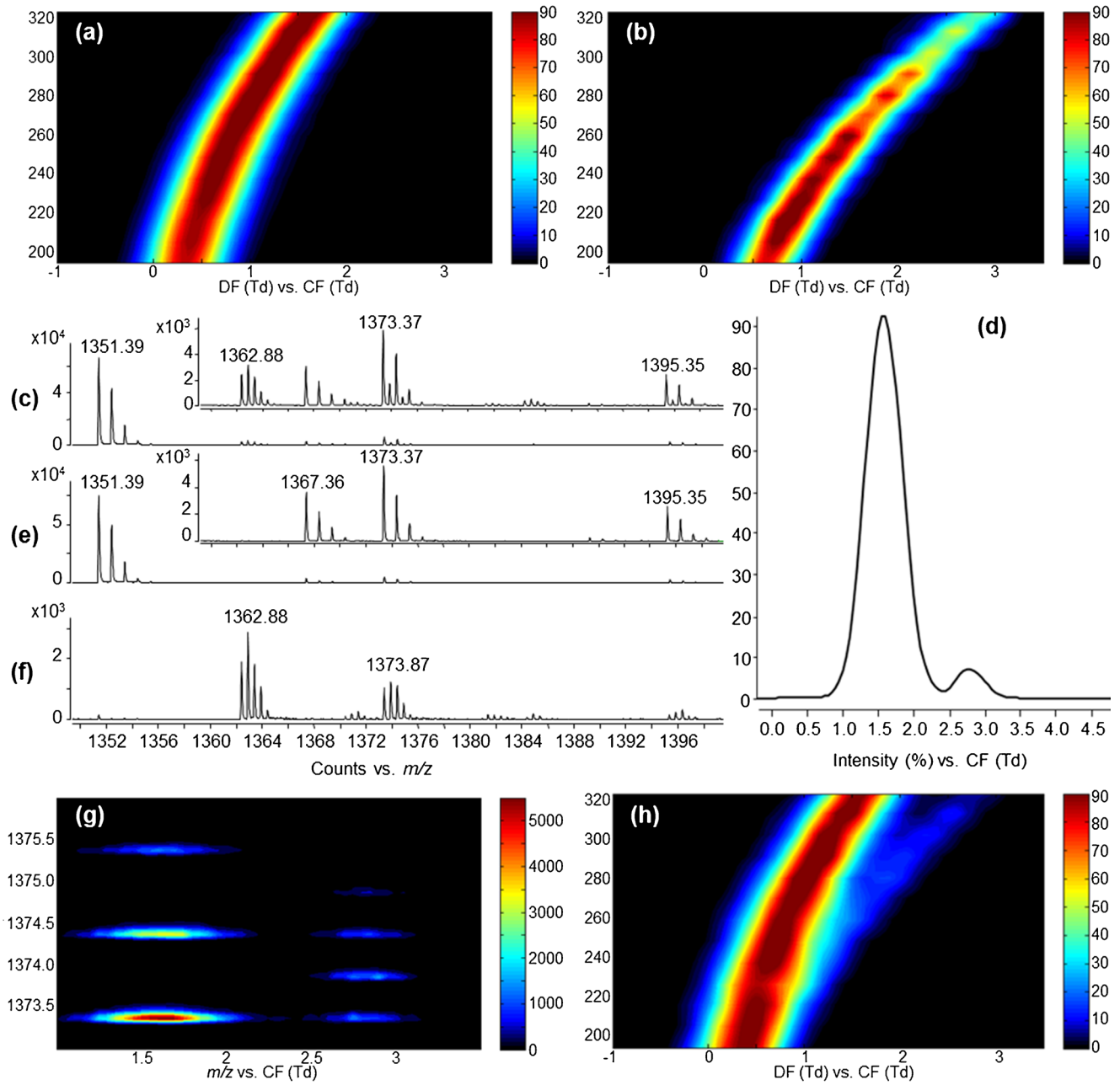

Figure 4. Overlapping charge state separation of 3-MX (+Na^+) complexes at fragmentor voltage of 150 V: three-dimensional heat maps of DF versus CF (with intensity (%) represented on the color scale) of (**a**) *m/z* 1351.38 ($[(3\text{-MX})_8 + Na]^+$) and (**b**) *m/z* 1362.38 ($[(3\text{-MX})_{16} + 3Na - H]^{2+}$); (**c**) mass spectrum with no FAIMS; (**d**) FAIMS CF scan at DF 323 Td, selected ion responses for *m/z* 1373.37; (**e**) FAIMS selected mass spectrum of singly charged species at DF 323 Td, CF 1.7 Td; and (**f**) FAIMS selected mass spectrum of doubly charged species at DF 323 Td, CF 2.85 Td; (**g**) three-dimensional heat map of *m/z* versus CF (at DF 323 Td, with intensity (%) represented on the color scale) showing the FAIMS separation of two isobaric species at *m/z* 1373.37, $[(3\text{-MX})_8 + 2Na - H]^+$ and $[(3\text{-MX})_{16} + 4Na - 2H]^{2+}$, and their isotopic patterns; (**f**) three-dimensional heat map of DF versus CF (with intensity (%) represented on the color scale) of *m/z* 1373.37 ($[(3\text{-MX})_8 + 2Na - H]^+$ and $[(3\text{-MX})_{16} + 4Na - 2H]^{2+}$

However, ESI-FAIMS-MS allows for the separation of ions based upon compound-dependent differences in high and low field mobility as a result of charge state [33, 36, 41]. FAIMS separation may therefore be used to suppress or enhance the transmission of singly or multiply charged ions selectively. The significance of this becomes apparent for overlapping isotopic patterns of singly and doubly charged species, such as $(3\text{-MX})_8$ and $(3\text{-MX})_{16}$ in the range *m/z* 1300–1400 in Figure 4c, which cannot be resolved by the reflectron TOF mass analyzer alone. However, the singly charged $[(3\text{-MX})_8 + 2Na - H]^+$ ion (*m/z* 1373.37) is resolved from the corresponding doubly charged $[(3\text{-MX})_{16} + 4Na - 2H]^{2+}$ ion with the same *m/z* by FAIMS (Figure 4d). FAIMS-selected transmission of the appropriate charge state is shown in Figure 4e and f, at CF 1.70 Td and 2.85

Td, respectively (DF 323 Td), resulting in the ESI-FAIMS-MS separation of overlapping singly and doubly charged isobaric 3-MX species in the mass spectrum. The most abundant octameric species with a single sodium cation ($[(3\text{-MX})_8 + Na]^+$) at *m/z* 1351.39 also demonstrates the ability of FAIMS to increase the signal-to-noise ratio (S:N), by 2.8 times in Figure 4e compared with the FAIMS off mass spectrum in Figure 4c, and also the ability to filter out this highly abundant singly charged species to reveal that there is no evidence of a $[(3\text{-MX})_{16} + 2Na]^{2+}$ complex, which would have the same *m/z* (Figure 4f). A 2- to 3-fold enhancement of the S:N was observed for all of the complexes in Figure 4e and f, compared with Figure 4c, as a result of the removal of background noise from the doubly and singly charged species for Figure 4e and f respectively.

In this study of 3-MX complexes, a second type of heat map of *m/z* versus CF at a particular DF (instead of DF versus CF at a particular *m/z*, as shown in Figure 2 and Figure 3) provides an alternative view of selected ions. Figure 4g is an example of such a plot, for *m/z* versus CF at DF 323 Td in the region *m/z* 1373-1376, which shows the FAIMS separation of the two isobaric species of *m/z* 1373.37, which correspond to the singly and doubly charged species $[(3\text{-MX})_8 + 2Na - H]^+$ and $[(3\text{-MX})_{16} + 4Na - 2H]^{2+}$. These isobaric singly and doubly charged species at *m/z* 1373.37 can also be plotted as a heat map of DF versus CF at all DFs, Figure 4h, which shows an intense peak corresponding to the singly charged $[(3\text{-MX})_8 + 2Na - H]^+$ and a secondary peak that begins to separate from the main intense peak at DF 240 Td and above. This heat map can be compared with those that are either singly or doubly charged with no corresponding peak present, such as those of *m/z* 1351.38 and 1362.38 (Figure 4a and b), demonstrating the similar profiles of the singly and doubly charged complexes.

The ESI-mass spectrum of 3-MX with sodium hydroxide as the solvent modifier (Figure 1e) is dominated by tetrameric complexes, and the transmission of some lower abundance non-tetrameric 3-MX isobaric species can be masked by these prominent ions (Figure 5). For example, in the mass spectrum of 3-MX in the region *m/z* 1016–1026 without FAIMS applied (Figure 5a), the peak at *m/z* 1019.3 could correspond to $[(3\text{-MX})_6 + Na]^+$ or $[(3\text{-MX})_{12} + 2Na]^{2+}$, though the isotope pattern suggests that only the doubly charged tetrameric species is present. However, comparison of the FAIMS peaks for the first two isotopes of this species (Figure 5b) at *m/z* 1019.28 and 1019.78 shows a small shoulder is observed at the low CF edge of the peak for *m/z* 1019.28. Careful selection of the FAIMS DF and CF makes it possible to filter out the (35 times) more abundant doubly charged species in order to selectively

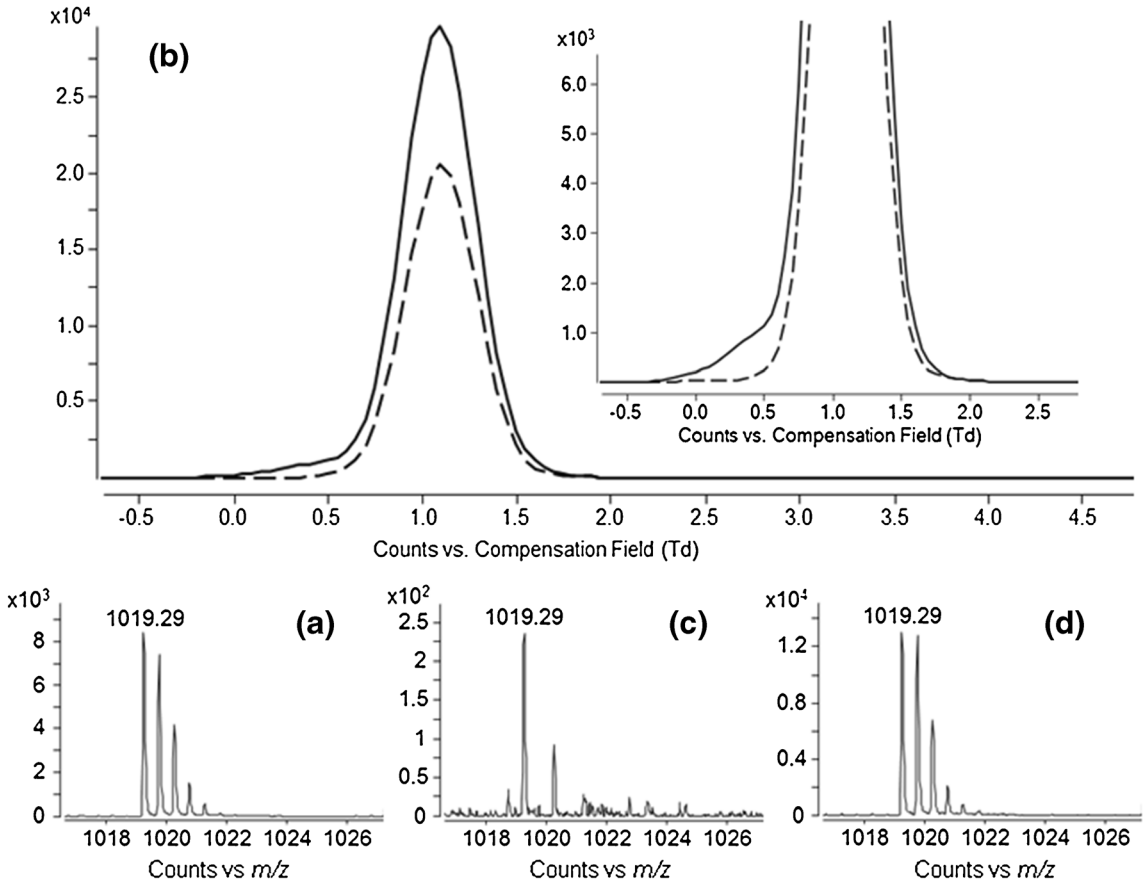

Figure 5. ESI-FAIMS-MS analysis of *m/z* 1019.28: (**a**) mass spectrum with no FAIMS applied; (**b**) FAIMS CF scan at DF 216 Td for *m/z* 1019.28 (solid line) and *m/z* 1019.78 (dotted line); (**c**) FAIMS selection of singly charged species (DF 216 Td, CF 0.25 Td); and (**d**) FAIMS selection of doubly charged species (DF 216 Td, CF 1.10 Td)

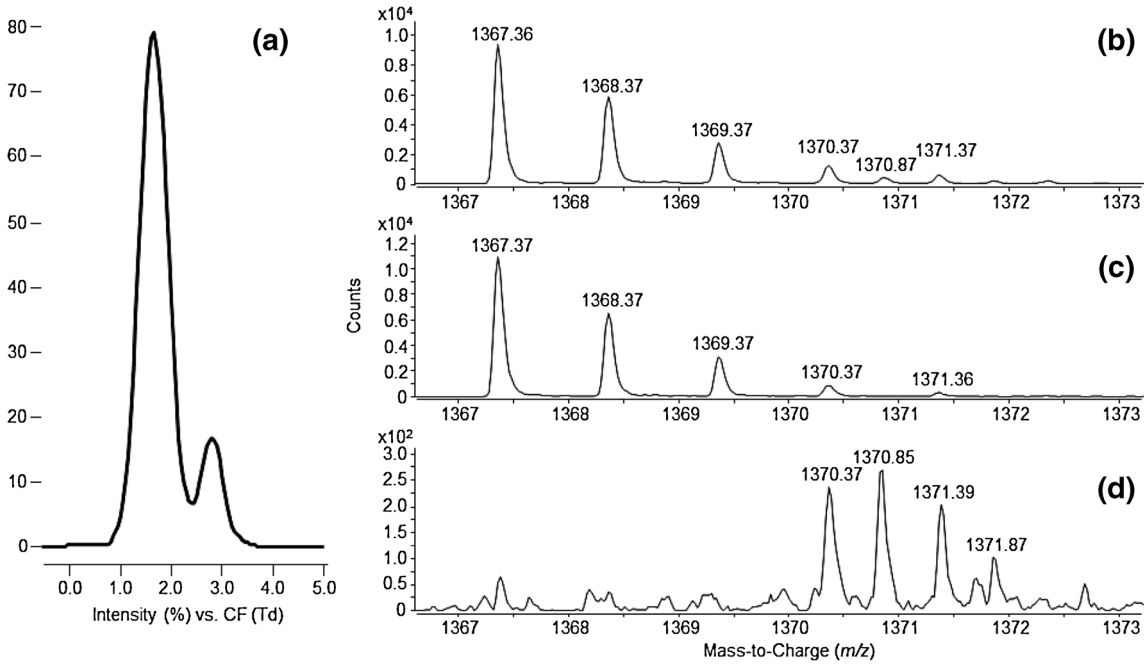

Figure 6. ESI-FAIMS-MS analysis of a hetero-cation $[(3\text{-MX})_{16} + 2Na + K - H]^{2+}$ of *m/z* 1370.36: (**a**) FAIMS CF scan at DF 323 Td; (**b**) mass spectrum with no FAIMS applied; (**c**) FAIMS selection at CF 1.65 Td; (**d**) FAIMS selection at CF 2.75 Td

transmit the singly charged $[(3\text{-MX})_6 + Na]^+$ ion (Figure 5c); without FAIMS separation it was not possible to determine the presence of this hexameric complex of 3-MX, whilst the tetrameric doubly charged $[(3\text{-MX})_{12} + 2Na]^{2+}$ dominates the mass spectrum. Also, by selecting the FAIMS at the maximum CF for transmission for *m/z* 1019.3 ($[(3\text{-MX})_{12} + 2Na]^{2+}$) at DF 216 Td, the S:N is doubled by reducing background noise in the mass spectrum (Figure 5d).The ability of FAIMS to investigate self-assembling supramolecular complexes of 3-MX doped with sodium has been demonstrated. However, ESI-FAIMS-MS analysis can also be used to investigate complexes of 3-MX with different stabilising cations NH_4^+, Na^+, and K^+ (Supplementary Figure 5) whose FAIMS conditions have been shown to vary dependent on cation. A combination of these varying FAIMS conditions and charge state separation has been utilised to identify hetero-cationized complexes of 3-MX (Figure 6). In the region *m/z* 1340–1450, a range of both singly and doubly charged complexes with different stabilising cations can be identified using ESI-FAIMS-MS that were previously hidden using ESI-MS alone. Figure 6 shows an example of how FAIMS can be used to separate these isobaric compounds of different charge state by examining the FAIMS CF spectra for *m/z* 1370.4 (Figure 6a). The mass spectral peak for *m/z* 1370.4 without FAIMS applied (Figure 6b) is an overlap of the more abundant $[(3\text{-MX})_8 + K]^+$ isotope peaks and a hidden doubly charged ion. Careful selection of the CF maxima of the two peaks in the FAIMS spectra (Figure 6a) and extraction of the mass spectra (Figure 6c and d) allows for the separation of the isobaric abundant singly charged complex, $[(3\text{-MX})_8 + K]^+$, and the doubly charged hetero-cationic complex, corresponding to $[(3\text{-MX})_{16} + 2Na + K - H]^{2+}$.

Complexes with multiple cations, both homo- and hetero-cationized complexes, appear to be stable with sodium cations even with ammonium acetate as the modifier. Singly charged octameric homo-cation complexes of 3-MX with up to five Na^+ were observed (DF 323 Td, CF 1.65 Td), whereas only $[(3\text{-MX})_8 + NH_4]^+$ and $[(3\text{-MX})_8 + K]^+$ were observed for NH_4^+ and K^+. Furthermore, the hetero-cation complexes with $Na^+ + K^+$ were more abundant than the $NH_4^+ + Na^+$ and $NH_4^+ + K^+$ complexes, with a range of $Na^+ + K^+$ complexes observed in the region *m/z* 1340–1450, for example $[(3\text{-MX})_8 + 3Na + K - 3H]^+$ (DF 323 Td, CF 1.65 Td) and $[(3\text{-MX})_{16} + 2Na + 2K - 2H]^{2+}$ (DF 226 Td, CF 0.85 Td). Hetero-cation complexes with all three cations were also observed, with very low intensities, which correspond to $[(3\text{-MX})_8 + NH_4 + Na + K - 2H]^+$ (*m/z* 1406.36; DF 323 Td, CF 2.75 Td), $[(3\text{-MX})_{16} + NH_4 + 2Na + K - 2H]^{2+}$ (*m/z* 1378.87; DF 313 Td, CF 2.60 Td), $[(3\text{-MX})_{16} + 3NH_4 + Na + 2K - 4H]^{2+}$ (*m/z* 1403.88; DF 216 Td, CF 0.80 Td), and $[(3\text{-MX})_{16} + NH_4 + 3Na + 2K - 4H]^{2+}$ (*m/z* 1408.84; DF 302 Td, CF 2.30 Td).

Conclusion

Miniaturized chip-based FAIMS combined with TOF MS has been applied to the study of self-assembling supramolecular noncovalent complexes of 3-MX. Noncovalently bound supramolecular complexes are shown to be able to successfully traverse the FAIMS device, but at high DFs there is evidence for in-FAIMS dissociation of higher ordered complexes may be observed. Singly charged 3-MX complexes of a tetrameric structure were shown to have different CF values for maximum

transmission, with CF decreasing with increasing complex size. FAIMS selection prior to mass analysis allows the separation of charge states of 3-MX complexes. Singly charged tetrameric complexes were found to be stable through the FAIMS device, even up to the highest DF values, whilst the doubly charged tetrameric species show a clear decline in intensity at higher CF values as the DF increases than singly charged 3-MX complexes. FAIMS preselection allows complexes that were previously concealed by more abundant overlapping isobaric species to be observed, further highlighting the complexity and depth of information that ESI-FAIMS-MS analysis can unravel in the study of these supramolecular complexes. ESI-FAIMS-MS has also been applied to an array of supramolecular noncovalent complexes of 3-MX with multiple cations present, and shown to aid in the identification of hetero-cation complexes. The hyphenation of ESI-FAIMS-MS has shown the potential to aid in the deconvolution of complicated mass spectra of other supramolecular noncovalent complexes.

Acknowledgments

The authors thank Owlstone Ltd., Agilent Technologies, and Loughborough University for financial support. The authors also thank Owlstone Ltd. and Agilent Technologies for the provision of instrumentation.

References

1. Lehn, L.M.: Toward complex matter: supramolecular chemistry nd self-organization. PNAS **99**, 4763–4768 (2002)
2. Lawrence, D.S., Jiang, T., Levett, M.: Self-assembling supramolecular complexes. Chem. Rev. **95**, 2229–2260 (1995)
3. Capito, R.M., Azevedo, H.S., Velichko, Y.S., Mata, A., Stupp, S.I.: Self-assembly of large and small molecules into hierarchically ordered sacs and membranes. Science **319**, 1812–1816 (2008)
4. Branco, M.C., Schneider, J.P.: Self-assembling materials for therapeutic delivery. Acta Biomater. **5**, 817–831 (2009)
5. Ciesielski, A., Haar, S., Benyei, A., Paragi, G., Guerra, C.F., Bickelhaupt, F.M., Masiero, S., Szolomajer, J., Samori, P., Spada, G.P., Kovacs, L.: Self-assembly of N3-substituted xanthines in the solid state and at the solid-liquid interface. Langmuir **29**, 7283–7290 (2013)
6. Lin, Y., Boker, A., He, J., Sill, K., Xiang, H., Abetz, C., Li, X., Wang, J., Emrick, T., Long, S., Wang, Q., Balazs, A., Russell, T.P.: Self-directed self-assembly of nanoparticle/copolymer mixtures. Nature **434**, 55–59 (2005)
7. Barbera, J., Donnio, B., Gehringer, L., Guillon, D., Marcos, M., Omenat, A., Serrano, J.L.: Self-organization of nanostructured functional dendrimers. J. Mater. Chem. **15**, 4093–4105 (2005)
8. Tirado, J.D., Acevedo, D., Bretz, R.L., Abruna, H.D.: Adsorption dynamics of electroactive self-assembling molecules. Langmuir **10**, 1971–1979 (1994)
9. Parviz, B.A., Ryan, D., Whitesides, G.M.: Using self-assembly for the fabrication of nano-scale electronic and photonic devices. IEEE Trans. Adv. Packag. **26**, 233–241 (2003)
10. Szolomájer, J., Paragi, G., Batta, G., Guerra, G.F., Bickelhaupt, F.M., Kele, Z., Padar, P., Kupihar, Z., Kovacs, L.: 3-Substituted xanthines as promising candidates for quadruplex formation: computational, synthetic and analytical studies. New J. Chem. **35**, 476–482 (2011)
11. Mezzache, S., Alves, S., Paumard, J.P., Pepe, C., Tabet, J.C.: Theoretical and gas-phase studies of specific cationized purine base quartet. Rapid Commun. Mass Spectrom. **21**, 1075–1082 (2007)
12. Sen, D., Gilbert, W.: Formation of parallel four-stranded complexes by guanine-rich motifs in DNA and its implications for meiosis. Nature **334**, 364–366 (1988)
13. Low, J.N., Tollin, P., Brand, E., Wilson, C.C.: Structure of 3-methylxanthine. Acta Crystallogr. **C42**, 1447–1448 (1986)
14. Geraets, L., Moonen, H.J., Wouters, E.F., Bast, A., Hageman, G.J.: Caffeine metabolites are inhibitors of the nuclear enzyme poly(ADP-ribose)polymerase-1 at physiological concentrations. Biochem. Pharmacol. **72**, 902–910 (2006)
15. Orlando, R., Padrini, R., Perazzi, M., De Martin, S., Piccoli, P., Palatini, P.: Liver dysfunction markedly decreases the inhibition of cytochrome P450 1A2-mediated theophylline metabolism by fluvoxamine. Clin. Pharmacol. Ther. **79**, 489–499 (2006)
16. Zydron, M., Baranowski, J., Baranowska, I.: Separation, pre-concentration, and HPLC analysis of methylxanthines in urine samples. J. Sep. Sci. **27**, 1166–1172 (2004)
17. Song, J., Park, K.U., Park, H.D., Yoon, Y., Kim, J.Q.: High-throughput liquid chromatography-tandem mass spectrometry assay for plasma theophylline and its metabolites. Clin. Chem. **50**, 2176–2179 (2004)
18. Rasmussen, B.B., Brosen, K.: Determination of theophylline and its metabolites in human urine and plasma by high-performance liquid chromatography. J. Chromatogr. B **676**, 169–174 (1996)
19. Safranow, K., Machoy, Z.: Simultaneous determination of 16 purine derivatives in urinary calculi by gradient reversed-phase high-performance liquid chromatography with UV detection. J. Chromatogr. B **819**, 229–235 (2005)
20. Hardin, C.C., Henderson, E., Watson, T., Prosser, J.K.: Monovalent cation induced structural transitions in telomeric DNAs: G-DNA folding intermediates. Biochemistry **30**, 4460–4472 (1991)
21. Yurenko, Y.P., Novotny, J., Sklenar, V., Marek, R.: Exploring noncovalent interactions in guanine- and xanthine-based model DNA quadruplex structures: a comprehensive quantum chemical approach. Phys. Chem., Chem. Phys. **16**, 2072–2084 (2014)
22. Ferreira, R., Marchand, A., Gabelica, V.: Mass spectrometry and ion mobility spectrometry of G-quadruplexes. A study of solvent effects on dimer formation and structural transitions in the telomeric DNA sequence d(TAGGGTTAGGGT). Methods **57**, 56–63 (2012)
23. Rosu, F., Gabelica, V., Poncelet, H., De Pauw, E.: Tetramolecular G-quadruplex formation pathways studied by electrospray mass spectrometry. Nucleic Acids Res. **38**, 5217–5225 (2010)
24. Baker, E.S., Bernstein, S.L., Bowers, M.T.: Structural characterization of G-quadruplexes in deoxyguanosine clusters using ion mobility mass spectrometry. J. Am. Soc. Mass Spectrom. **16**, 989–997 (2005)
25. Paragi, G., Kovacs, L., Kupihar, Z., Szolomajer, J., Penke, B., Guerra, C.F., Bickelhaupt, F.M.: Neutral and positively charged new purine tetramer structures: a computational study of xanthine and uric acid derivatives. New J. Chem. **35**, 119–126 (2011)
26. Mautjana, N.A., Looi, D.W., Eyler, J.R., Brajter-Toth, A.: Sensitivity of positive ion mode electrospray ionization mass spectrometry (ESI MS) in the analysis of purine bases in ESI MS and on-line electrochemistry ESI MS (EC/ESI MS). Electrochim. Acta **55**, 52–58 (2009)
27. Eiceman, G.A., Karpas, Z.: Ion Mobility Spectrometry, 2nd edn. CRC Press, Boca Raton (2005)
28. Shvartsburg, A.A.: Differential Ion Moblity Spectrometry: Non-Linear Ion Transport and Fundamentals of FAIMS. CRC Press, Boca Raton (2009)
29. Kolakowski, B.M., Mester, Z.: Review of applications of high-field asymmetric waveform ion mobility spectrometry (FAIMS) and differential mobility spectrometry (DMS). Analyst **132**, 842–864 (2007)
30. Guevremont, R.: High-field asymmetric waveform ion mobility spectrometry: a new tool for mass spectrometry. J. Chromatogr. A **1058**, 3–19 (2004)
31. Shvartsburg, A.A., Li, F., Tang, K., Smith, R.D.: High-resolution FAIMS using new planar geometry analyzers. Anal. Chem. **78**, 3706–3714 (2006)
32. Shvartsburg, A.A., Smith, R.D., Wilks, A., Koehl, A., Ruiz-Alsonso, D., Boyle, B.: Ultrafast differential ion mobility spectrometry at extreme electric fields in multichannel microchips. Anal. Chem. **81**, 6489–6495 (2009)
33. Brown, L.J., Toutoungi, D.E., Devenport, N.A., Reynolds, J.C., Kaur-Atwal, G., Boyle, P., Creaser, C.S.: Minaturized ultra high field asymmetric waveform ion mobility spectrometry combined with mass spectrometry for peptide analysis. Anal. Chem. **82**, 9827–9834 (2010)
34. Rorrer, L.C., Yost, R.A.: Solvent vapor effects in planar high-field asymmetric waveform ion mobility spectrometry: Solvent trends and temperature effects. Int. J. Mass Spectrom. **378**, 336–346 (2015)
35. Smith, R.W., Reynolds, J.C., Lee, S., Creaser, C.S.: Direct analysis of potentially genotoxic impurities by thermal desorption-field asymmetric

waveform ion mobility spectrometry-mass spectrometry. Anal. Methods **5**, 3799–3802 (2013)
36. Brown, L.J., Smith, R.W., Toutoungi, D.E., Reynolds, J.C., Bristow, A.W.T., Ray, A., Sage, A., Wilson, I.D., Weston, D.J., Boyle, B., Creaser, C.S.: Enhanced analyte detection using in-source fragmentation of field `asymmetric waveform ion mobility spectrometry—selected ion in combination with time-of-flight mass spectrometry. Anal. Chem. **84**, 4095–4103 (2012)
37. Smith, R.W., Cox, L.B., Yudin, A., Reynolds, J.C., Powell, M., Creaser, C.S.: Rapid determination of *N*-methylpyrrolidine in cefepime by combining direct infusion electrospray ionization-time-of-flight mass spectrometry with field asymmetric waveform ion mobility spectrometry. Anal. Methods **7**, 34–39 (2015)
38. Menlyadiev, M.R., Tarassov, A., Kielnecker, A.M., Eiceman, G.A.: Tandem differential mobility with ion dissociation in air at ambient pressure and temperature. Analyst **140**, 2995–3002 (2015)
39. MATLAB: Release 2014a. The MathWorks, Inc., Natick, Massachusetts (2014)
40. Guevremont, R., Purves, R.W.: High field asymmetric waveform ion mobility spectrometry-mass spectrometry: an investigation of leucine enkephalin ions produced by electrospray ionization. J. Am. Soc. Mass Spectrom. **10**, 492–501 (1999)
41. Brown, L.J., Creaser, C.S.: Field asymmetric waveform ion mobility spectrometry analysis of proteins and peptides: a review. Curr. Anal. Chem. **9**, 192–198 (2013)